

A Conformal FDTD Software Package Modeling Antennas and Microstrip Circuit Components

Wenhua Yu, Senior Member, IEEE, and Raj Mittra, Life Fellow, IEEE
Electromagnetic Communication Laboratory, 319 EE East
The Pennsylvania State University
University Park, PA 16802
wxy6@psu.edu and rjm53@psu.edu

1. Abstract: This paper describes a conformal Finite Difference Time Domain (FDTD) software package and presents its applications to RF antennas and microstrip circuit components. The program includes a Visual Basic GUI for graphically inputting the object geometries, setting source and boundary conditions, generating a non-uniform mesh, and post processing of the data. A robust Conformal Finite Difference Time Domain (CFDTD) technique is employed to handle conductors with curved surfaces and edges. Illustrative examples that show the application of the code for modeling antennas as well as microstrip discontinuities are presented in the paper.

Keywords: FDTD Method; Conformal FDTD Method; Mesh Generation; Software Package; Boundary Condition; GUI; Microstrip Circuits; Microstrip Components; Antennas, Cavity; Visual Language.

2. Introduction

The Finite Difference Time Domain (FDTD) method has been widely used to simulate various electromagnetic problems [1-10] because of its flexibility and versatility. Many variations and extensions of the FDTD exist, and the literature on the FDTD technique is extensive. In the past decade, most of the research on FDTD has focused on two challenging topics. The first of these is the development of accurate and computationally efficient absorbing boundary conditions to model open region problems, while the second one deals with the perfectly electrical conductors with curved surfaces and edges by using a conformal FDTD scheme. The Perfectly Matched Layer (PML), proposed by Berenger in 1994, is a highly accurate approach to mesh truncation [11], though it does increase the computational complexity and the memory requirement for the FDTD simulation; hence, the search for alternative boundary conditions continues unabated.

As for the conformal FDTD technique, it has over a ten-year history and there have been a large number of contributors on this topic. However, many of these approaches [12-15] require complicated distorted mesh information and, furthermore, often suffer from the late-time instability problem unless special cares are taken to ensure the stability, *e.g.*, by using a smaller time step than that dictated by the Courant condition. The authors recently proposed an efficient and accurate conformal FDTD (CFDTD) technique [16,17], which does not require significant modification of the Cartesian-type of FDTD and, hence, preserves the computational efficiency of the conventional FDTD technique. This CFDTD algorithm employs an update algorithm that uses the distorted edge lengths to account for the deformation of the FDTD cells containing the curved objects rather than distorted cell areas utilized in some of other CFDTD schemes.

The above CFDTD technique has been combined with the Visual Basic interface to develop an FDTD software package. It includes a graphical user interface for inserting the geometry, a built-in non-uniform mesh generator, and other features that include post processing

of the data. In the following, we describe the main parts of this software package and present its applications to some representative electromagnetic problems. It is well known that the Cartesian-grid FDTD technique, which has been successfully applied to solve a variety of electromagnetic problems, utilizes a cubic prism as the unit cell. Thus, it may produce significant errors when modeling perfect electric conductors (PECs) with curved surfaces and edges, owing to the staircasing approximation it introduces in the process. To illustrate the capability of the present software to handle curved PEC objects, all of the examples presented in this paper include perfect conductors with curved surfaces or edges.

3. Brief Review of Finite Difference Time Domain Techniques

3.1. Finite Difference Time Domain Method

In a pioneering paper, written in 1966 [1], Yee introduced a set of Finite-Difference representations for the time-dependent Maxwell's curl equations. In Yee's scheme, the computational domain is subdivided by using an orthogonal mesh in the Cartesian coordinate system. The electric fields are located along the edges of cells, while the magnetic fields are positioned at the centers of these cells. Maxwell's difference equations in the Yee scheme are written as:

$$H_x^{n+1/2}(i, j, k) = H_x^{n-1/2}(i, j, k) + \frac{\Delta t}{\mu_x(i, j, k)} \left(\frac{E_y^n(i, j, k+1) - E_y^n(i, j, k)}{\Delta z(k)} - \frac{E_z^n(i, j+1, k) - E_z^n(i, j, k)}{\Delta y(j)} \right) \quad (1)$$

$$H_y^{n+1/2}(i, j, k) = H_y^{n-1/2}(i, j, k) + \frac{\Delta t}{\mu_y(i, j, k)} \left(\frac{E_z^n(i+1, j, k) - E_z^n(i, j, k)}{\Delta x(i)} - \frac{E_x^n(i, j, k+1) - E_x^n(i, j, k)}{\Delta z(k)} \right) \quad (2)$$

$$H_z^{n+1/2}(i, j, k) = H_z^{n-1/2}(i, j, k) + \frac{\Delta t}{\mu_z(i, j, k)} \left(\frac{E_x^n(i, j+1, k) - E_x^n(i, j, k)}{\Delta y(j)} - \frac{E_y^n(i+1, j, k) - E_y^n(i, j, k)}{\Delta x(i)} \right) \quad (3)$$

$$E_x^{n+1}(i, j, k) = \frac{\varepsilon_x(i, j, k) - 0.5 \cdot \Delta t \cdot \sigma_x(i, j, k)}{\varepsilon_x(i, j, k) + 0.5 \cdot \Delta t \cdot \sigma_x(i, j, k)} E_x^n(i, j, k) + \frac{\Delta t}{\varepsilon_x(i, j, k) + 0.5 \cdot \Delta t \cdot \sigma_x(i, j, k)} \left(\frac{H_z^{n+1/2}(i, j+1, k) - H_z^{n+1/2}(i, j, k)}{\Delta y(j)} - \frac{H_y^{n+1/2}(i, j, k+1) - H_y^{n+1/2}(i, j, k)}{\Delta z(k)} \right) \quad (4)$$

$$E_y^{n+1}(i, j, k) = \frac{\varepsilon_y(i, j, k) - 0.5 \cdot \Delta t \cdot \sigma_y(i, j, k)}{\varepsilon_y(i, j, k) + 0.5 \cdot \Delta t \cdot \sigma_y(i, j, k)} E_y^n(i, j, k) + \frac{\Delta t}{\varepsilon_y(i, j, k) + 0.5 \cdot \Delta t \cdot \sigma_y(i, j, k)} \left(\frac{H_x^{n+1/2}(i, j, k+1) - H_x^{n+1/2}(i, j, k)}{\Delta z(k)} - \frac{H_z^{n+1/2}(i+1, j, k) - H_z^{n+1/2}(i, j, k)}{\Delta x(i)} \right) \quad (5)$$

$$E_z^{n+1}(i, j, k) = \frac{\varepsilon_z(i, j, k) - 0.5 \cdot \Delta t \cdot \sigma_z(i, j, k)}{\varepsilon_z(i, j, k) + 0.5 \cdot \Delta t \cdot \sigma_z(i, j, k)} E_z^n(i, j, k) + \frac{\Delta t}{\varepsilon_z(i, j, k) + 0.5 \cdot \Delta t \cdot \sigma_z(i, j, k)} \left(\frac{H_y^{n+1/2}(i+1, j, k) - H_y^{n+1/2}(i, j, k)}{\Delta x(i)} - \frac{H_x^{n+1/2}(i, j+1, k) - H_x^{n+1/2}(i, j, k)}{\Delta y(j)} \right) \quad (6)$$

where the superscripts represent the time index and the arguments correspond to spatial sampling locations. To avoid numerical instabilities, the time increment Δt must satisfy the Courant condition:

$$\Delta t \leq \frac{1}{c \sqrt{\left(\frac{1}{\Delta x}\right)^2 + \left(\frac{1}{\Delta y}\right)^2 + \left(\frac{1}{\Delta z}\right)^2}} \quad (7)$$

where, Δx , Δy , Δz are the lattice dimensions of the cells.

3.2. Perfectly Matched Layers (PML)

The concept of a Perfectly Matched Layer (PML) medium was introduced by Berenger in 1994. A unique character of the PML is that plane waves of arbitrary incidence, polarization, and frequency are matched at the boundary in a reflectionless manner. There are two different versions of the PML, *viz.*, split-field [11] and unsplit-field [18] formulations. Both of these produce a very low reflection when used to truncate the FDTD lattice, though the former requires less memory. In this software we use a 10-layer Unsplit Perfectly Matched Layer (UPML) for mesh truncation, which generates a very low level of reflection. In addition, this software provides an option to use PEC and PMC terminations, as well as the simpler (though less accurate than PML) Mur boundary condition.

3.3. Conformal FDTD Technique

If there are perfect conductors with curved surfaces and edges in the computational domain, as shown in Fig. 1, the staircasing approximation of the conventional FDTD technique may produce significant errors. To overcome this difficulty, we introduce a novel conformal FDTD algorithm [16,17] in this section. In this approach, we assume that both the electric and magnetic fields inside the distorted cell are located at the same positions as those in the conventional FDTD scheme and that Faraday's law is applied over the entire FDTD cell rather than only in the distorted part. This implies that the contour path follows the edges of the FDTD in its entirety. Because some parts of the contour path are located inside the PEC region, we discard the distribution of these segments and write the $\oint \vec{E} \cdot d\vec{l}$ contour integral, appearing in the representation for the H-field as follows:

$$\oint \vec{E} \cdot d\vec{l} = \left[\begin{array}{l} \int_{\Delta x_0(i)} E_x(i, j, k) \cdot dx + \int_{\Delta z_0(k)} E_z(i, j, k) \cdot dz \\ + \int_{\Delta x(i, j, k+1)} E_x(i, j, k+1) \cdot dx + \int_{\Delta z(i+1, j, k)} E_z(i+1, j, k) \cdot dz \end{array} \right] \quad (8)$$

The definitions of the variables used in above equation are shown in Fig. 2. Although the computation of the H -field is slightly modified in this manner, we leave the representation of the E -field unchanged from that in the conventional FDTD scheme. Using (8), the magnetic fields inside the partially-filled cells are updated by using a slightly different form of the conventional

FDTD algorithm which accounts for the deformation of the cell. The update equation for the H-field reads:

$$H_y^{n+1/2}(i, j, k) = H_y^{n-1/2}(i, j, k) + \frac{\Delta t}{\mu_y(i, j, k)} \times \left[\frac{\Delta z(i, j, k)E_z^n(i, j, k) - \Delta z(i-1, j, k)E_z^n(i-1, j, k)}{\Delta x_0(i) \times \Delta z_0(k)} + \frac{\Delta x(i, j, k-1)E_x^n(i, j, k-1) - \Delta x(i, j, k)E_x^n(i, j, k)}{\Delta x_0(i) \times \Delta z_0(k)} \right] \quad (9)$$

Note that unlike past approaches, we do not employ the deformed cell area for updating the H-field, but use the entire cell area instead (see Fig. 2); this, in turn, serves to eliminate the instability problems experienced in the past.

3.4. Near-to-Far-Zone Field Transformation

The FDTD algorithm can be computer-intensive and, to save memory and run times, it is necessary to use as small a computational domain as possible in the simulations. Then, to calculate the far zone field, it is necessary to combine the FDTD with the near-to-far zone field transformation algorithm [19]. The equivalent electric and magnetic currents on the closed Huygen's surface are computed by using the FDTD method, the far zone field is there obtained from these equivalent current sources. Because the electric and magnetic field locations have a half-cell separation in Yee's FDTD scheme, the fields on the Huygen's surface are derived by averaging. It is not desirable to store the electric and magnetic currents on the Huygen's surface for all of the time steps because that places an excessive burden on the memory resources; instead, we apply the DFT technique to transform the data from the time to frequency domains at each time step.

3.5. Handling the Interfaces Between Dissimilar Media

In the conventional FDTD scheme, the magnetic parameters of the medium, viz., $\mu_x, \mu_y, \mu_z, \sigma_x^*, \sigma_y^*$ and σ_z^* , are associated with the locations where the magnetic field components are sampled. The corresponding situation is also true for the locations of the electrical parameters, viz., $\epsilon_x, \epsilon_y, \epsilon_z, \sigma_x, \sigma_y$ and σ_z , and the electric fields. However, the above scheme is difficult to use in a complex FDTD domain, which may contain numerous interfaces, edges and corners. This is because special treatments are required on each interface, as well as at edges and corners, to satisfy the requisite boundary conditions. To circumvent this problem, we introduce an alternative scheme [20] in which the parameters of the media are defined at the centers of the FDTD cells, instead of at the locations of the fields. In the alternative scheme, the local value of the effective permittivity of the medium is calculated, before updating the fields, at the locations of the electric fields by taking an average of field values at the four points around the electric field location. Likewise, the effective permeability at the locations of the magnetic fields is derived by taking an average of the field values at points above and below these locations. This alternative scheme yields a universal formula which is valid both inside the uniform regions, as well as at the edges and corners.

4. Graphical User Interface (GUI)

In this section, we describe a graphical user interface developed by using Visual Basic [21], which is well known as a general-purpose developmental tool for such interfaces. We employ the Visual Basic software for automatically generating a non-uniform mesh needed in the FDTD algorithm. We also use the basic graphical functions available in Visual Basic, e.g., *point*, *line*, *rectangle* and *ellipse*, to model arbitrary objects in the FDTD simulations. Basic text input and output functions, such as *text box*, *combobox*, *listbox*, *val*, *scroll bar* and *label button*, serve to

input the boundary condition, source and output parameters. Graphical functions, such as *picture box* and *image box*, are used to plot object geometries and for mesh generation. *RichtextBox* is used to open, edit and save a text file, and *CommonDialog* is employed to control the color, font, and fill style of a picture. Certain control commands, e.g., *command button* and *radio button* are used to realize the control operations on the text and graphics. The title page of the software is displayed in Fig. 3.

4.1. Graphical Object Input

The control commands in Visual Basic allow us to build the relationship between the text and graphical functions. We input the object geometries and constitutive parameters in a *text box*, use the graphical functions to draw the object in the picture region, edit its color and fill its style by using the options provided in *CommonDialog*. In Visual Basic, *CommonDialog* is used to carry out certain simple tasks, such as loading and saving files, selecting directory, printing picture and text, choosing object color and fill style. For a given view angle ϕ , we project a three-dimensional object on a two-dimensional plane, and calculate the corresponding length in this plane. Assuming that the coordinates in the three dimensional space are (x', y', z') , the coordinates (x, z) in the picture window (x - z plane) are written as:

$$\begin{bmatrix} x + x_0 \\ z + z_0 \end{bmatrix} = \begin{bmatrix} 1 & \cos \phi & 0 \\ 0 & \sin \phi & 1 \end{bmatrix} \begin{bmatrix} x' \\ y' \\ z' \end{bmatrix}$$

where (x_0, z_0) is the position of the original point in the picture window. We change the viewing direction by selecting different view angles ϕ . The original position (x_0, z_0) controls the relative position of the picture in the picture window. In this software, we employ several basic graphical shapes, such as rectangles, cylinders, ring cylinders and hollow cylinders, for geometry modeling. By combining these, we can model arbitrary geometries arising in most applications. Figure 4, which shows the configuration of an annular microstrip resonator mounted on a substrate, serves to illustrate of this point.

4.2. Graphical Mesh Generation

For graphical mesh generation, we divide the FDTD domain into a number subregions bounded by the object borders [22]. The mesh in each subdomain may either be uniform or non-uniform depending upon the nature of the problem. However, a smooth transition between the two adjacent subregions is required to minimize reflection from the non-uniform mesh. In this software, these mesh parameters in the FDTD domain can be arranged graphically.

In each subregion, the cell size, ratio and domain size satisfy the following relationship:

$$\Delta_0 + \Delta_1 + \Delta_2 + \Delta_3 + \cdots + \Delta_{n-1} = L \quad (10)$$

where $\Delta_i = \alpha^i \cdot \Delta_0$ is the i^{th} cell size, whereas α and L are the ratio and the subregion length, respectively. In the mesh generation window, we select the ratio α and the minimum Δ_0 to realize the desired mesh distribution in each region. The subregion size, maximum cell size, the cell number in the subregion are also shown in this window. Figure 5 shows a simple mesh window.

4.3. Connection Between C++ and Visual Basic

We can directly run the conformal mesh and FDTD executable files from the graphical user interface by clicking the corresponding buttons in the toolbar. Visual Basic uses a *Shell* function to call a DOS executable file. For example, to run the conformal mesh and the FDTD executable files, we use the commands *Shell('CMESH.EXE', 1)* and *Shell('FDTD.EXE', 1)*, respectively. The

number “1” inside the parenthesis means that if the call for the DOS executable file fails, an error message will be returned on the screen.

4.4. Conformal Mesh Generation

If the FDTD domain includes PEC objects with curved surfaces and edges, we need to call the conformal mesh code from the graphical user interface to compute the geometrical parameters needed to deal with the distorted cells. The geometry information of the curved surfaces and edges of objects placed in a uniform or non-uniform mesh is used to calculate the distorted cell sizes located outside the PEC region for use in the conform mesh code. Because the information on the areas of these cells is not required in the present conformal FDTD technique, the calculation of the distorted cell lengths is quite simple.

4.5. Handling Data File name and Paths

In developing the graphical user interface, one of the important steps entails the inputting and storing of data file paths and names. The input file, output file, and the executable files are sorted in different subdirectories. These files and paths are placed in a text list file. This list file is located in the specific directory, for instance, the directory of the interface folder. When we click on the executable button in the toolbar to run the executable file, the FDTD code automatically recognizes the input and output paths and names specified in the interface. Visual Basic enables us to open a file and to save file path and name by using *commonDialog* control. For example, when we use the file and path window to save or open a file, the entire file path name is automatically stored in *CommonDialog.FileName*, e.g., *CommonDialog.FileName* = “C:/FDTD/geometry/input.dat.” *CommonDialog.Filter* = “Data File(*.dat)|*.dat|All file(*.*)|*.*” shows the file formats in the opening and saving window, *commonDialog.DefaultExt* = “dat” shows the default extension file name in the current opening and saving window, and *commonDialog.ShowOpen* and *commonDialog.ShowSave* control the save and open options, respectively.

One typical string operation example is shown in the following subroutine. Its purpose is used to determine how many lines and columns are contained in a data file which is chosen by the user from the interface.

```
Private Sub openfileforplot_Click()
    Dim a, b, temp_string, temp as string
    Dim i, j, n1, n2, n, nn as integer
    With CommonDialog
        .Filter = "Data File(*.dat)|*.dat|All file(*.*)|*.*"
        .DefaultExt = "dat"
        .Showopen
    End With

    If CommonDialog.FileName = "" Then Exit Sub
    On Error GoTo fileerror
    Open CommonDialog.FileName For Input As #1
    Line Input #1, temp_string
    temp_string = Trim(temp_string)
    n = 0 // the number of column in the data file
    j = 1
    For i = 1 To Len(temp_string)
        a = Left(temp_string, i)
```

```

    B = Left(temp_string, i + 1)
    n1 = Len(Trim(a))
    n2 = Len(Trim(B))
    If n1 = n2 Then
        n = n + 1
        If j = i - 1 Then
            n = n - 1
        End If
        j = i
    End If
Next i
If n = 0 Then
    Message_box = MsgBox("Wrong format or void file !", , "Warning")
    Exit Sub
End If
i = 1
While Not EOF(1)
    Line Input #1, temp$
    i = i + 1
Wend: Close #1
nn = i - 1 // the number of line in the data file

ReDim data_file(nn, n)

Open CommonDialog.FileName For Input As #1
For i = 0 To nn - 1
    For j = 1 To n
        Input #1, data_file(i, j) // store the data in the data_file

    Next j
Next i
Close #1

fileerror:
    Select Case Err.Number
    Case 52
        MsgBox "your file name is invalid"
        Exit Sub
    Case 53
        MsgBox "can not find file"
        Exit Sub
    Case 57
        MsgBox "An I/O device error has occurred"
        Exit Sub
    End Select
End Sub

```

In order to edit a data file from the interface, we need to use the *RichTextBox* control and its two options, *i.e.*, *Loadfile* and *Savefile*. For example, “*RichTextBox_editfile.LoadFile filename*” loads a data file into a *richtextbox* and “*RichTextBox_editfile.SaveFile filename 1*” (1: text file ; 0: rtf file) saves the edited data file.

5. Illustrative Examples

In this section, we present some examples to illustrate the application of this software to the simulation of a number of representative electromagnetic problems, all of which include a PEC object with a curved surface or an edge. For the excitation, we use a Gaussian pulse modulated by a sine function, and employ a 10-layer unsplit PML [18] to truncate the FDTD domain at the open boundaries. The time step is chosen to be:

$$\Delta t = \frac{0.995}{c \sqrt{\left(\frac{1}{\Delta x}\right)^2 + \left(\frac{1}{\Delta y}\right)^2 + \left(\frac{1}{\Delta z}\right)^2}} \quad (11)$$

Note that the above time step is very close to that dictated by the Courant condition for the regular undistorted cell, and is not geared to the size of the smallest distorted cell, which would make the time step much smaller and the computation time will correspondingly increase. The main steps followed in the simulation of the an electromagnetic problem is given below:

- (1) Input object geometries in the graphical user interface window (see Fig. 4);
- (2) Select boundary condition (absorbing boundary condition, PEC or PMC), output parameters, excitation source property and locations through corresponding dialogs;
- (3) Generate uniform or non-uniform mesh using the graphical mesh generation window;
- (4) Run the conformal mesh code if the FDTD domain includes PEC objects with curved surfaces and edges;
- (5) Run the CFDTD code;
- (6) Open the drawing window to plot the results obtained from the CFDTD simulation.

5.1. Quarter Wave Monopole Mounted on A PEC Disk

We consider a quarter-wavelength monopole mounted on a perfectly conducting elliptic disk, as shown in Fig. 6. The field in the shadow region of the elliptic disk is produced by diffraction from the curved edges of the disk. The surfaces of the Huygen’s box for the near-to-far zone field transformation are located five cells away from the boundary, and from the edge of the disk. The major and minor axes of the elliptic disk (b and a) are 1.7 and 1.5 meters, respectively. A Gaussian pulse with a 3-dB cutoff frequency at 300 MHz is modulated by a sine function (300 MHz). A z -polarized electric field source is located at the gap ($\lambda/20$) between the monopole and the elliptic disk. The FDTD domain includes $79 \times 87 \times 30$ cells with a uniform mesh $dx = 0.05 \text{ m}$, $dy = 0.05 \text{ m}$ and $dz = 0.05 \text{ m}$. The normalized far zone field patterns for both $\phi = 0^\circ$ and $\phi = 90^\circ$ at a frequency of 300 MHz are shown in Fig. 7 and Fig. 8. The result has been obtained by using 4048 time steps. We observe that they are in good agreement with those derived by using the MoM technique.

To test the validity of the CFDTD scheme on a non-uniform mesh, we use this software to calculate the far zone field pattern for the aforementioned geometry, but with a circular disk ($a = 0.62 \text{ m}$ and $b = 0.62 \text{ m}$). A fine mesh is used around the monopole, and in the vicinity of the edges of the disk as well. The entire FDTD domain includes $83 \times 83 \times 30$ cells, the minimum and maximum cell edge lengths are 0.015 m ($\lambda/20$) and 0.023 m ($\lambda/8$) in the x - and y -directions, and the numbers are $100 \times 100 \times 30$ for the uniform mesh domain. The ratio of adjacent cell

edge lengths within the non-uniform regions is 1.03. A uniform mesh is used in the z -direction with $dz = 0.015 \text{ m}$ ($\lambda/20$). The result has been obtained by using 4048 time steps. The normalized far zone field pattern at a frequency of 1 GHz is shown in Fig. 9. Additional runs have been made, going up to 15,000 time steps, and no instability has ever been observed. Once again, we note that the conformal FDTD results are in good agreement with those obtained from analytical methods.

5.2. Cylindrical Cavity

For the second example, we use the software to calculate the resonant frequencies of the dominant TE and TM modes for circularly-cylindrical cavities. The results for the resonant frequencies are shown in Table I, together with the dimensions of the cavities, with R and H representing the radius and height of the cylindrical cavities. The spatial discretization is chosen to be 0.005 m for each of the four cases studied, and the results have been obtained by using 8192 time steps. We observe good agreement between the conformal FDTD results and those obtained analytically. Additional runs have been made, going up to 40,000 time steps and once again no instability has ever been observed.

Table I. Comparison of resonant frequencies of a circularly-cylindrical cavity derived by using the analytical and CFDTD techniques

Modes	Methods	Geometry I R×H= (0.1m×0.1m)	Geometry II R×H= (0.1m×0.08m)	Geometry III R×H= (0.1m×0.06m)	Geometry IV R×H= (0.06m×0.06m)
TE ₁₁₁	CFDTD	1.734	2.062	2.639	3.133
	Analytical	1.738	2.071	2.650	3.148
	Difference	0.23%	0.43%	0.42%	0.48%
TM ₀₁₁	CFDTD	1.88	2.194	2.742	2.872
	Analytical	1.889	2.199	2.751	2.897
	Difference	0.48%	0.23%	0.33%	0.86%

5.3. Monolithic Microwave Integrated Circuits

In this section, we simulate four representative planar microwave circuits by using the above CFDTD technique to illustrate its ability to handle complex MMIC structures. These include a radial stub, a microstrip-coupled circular patch antenna, an annular microstrip resonator and a coupled annular microstrip resonator. The results obtained from the CFDTD technique are compared with the experimental data, and good agreement is observed for all of these examples.

5.3.1. Radial Stub

First, we consider a radial stub closely coupled with microstrip lines and discontinuities, as shown in Fig. 10. The circular shape of the radial stub is modeled by using the CFDTD technique described in section 3.3. The dimensions of the computational domain are $8.12 \times 8.12 \times 0.889 \text{ mm}^3$ and the domain is discretized into $40 \times 40 \times 7$ cells. In order for the edges of the microstrip lines to coincide with those of the FDTD grid, we choose a non-uniform mesh whose dimensions are: $\Delta x(i) = 0.20175 \text{ mm}$, $i = 1, 2, 3, 4$, $\Delta x(i) = 0.203357 \text{ mm}$, $i = 5, \dots, 18$, $\Delta x(i) = 0.203 \text{ mm}$, $i = 19, 20, 21$, $\Delta x(i) = 0.20333 \text{ mm}$, $i = 26, \dots, 36$, and $\Delta x(i) = 0.20175 \text{ mm}$, $i = 37, 38, 39, 40$. A uniform mesh is used in the z -direction with a cell dimension of $\Delta z(k) = 0.127 \text{ mm}$. A voltage source is placed between the ground plane and the left microstrip line at a distance of five cells away from the domain boundary ($y = 0$), while the observation point is located at a

distance of ten cells away from the boundary ($y = y_{max}$) in the y -direction. The 3 dB cut-off frequency of the excitation source is 25 GHz. The simulation is run for 8,192 time steps, with a time step of $\Delta t = 0.3146$ ps, and the solution is found to be entirely stable. The scattering parameter S_{21} vs. frequency is shown in Fig. 11. Good agreement with the experimental data, reported in [23], is observed. In addition, no instabilities are detected, even though the program has been tested up to 40,000 time steps.

5.3.2. Microstrip Patch Antenna

Next, we compute the scattering parameter of a microstrip patch antenna of circular shape, as shown in Fig. 12. The dimensions of the computational domain are $0.11 \times 0.088 \times 0.00795$ m³ and are subdivided into $55 \times 44 \times 10$ cells. The cell dimensions are chosen to be 0.002 m, 0.002 m and 0.000795 m, in the x -, y - and z -directions, respectively. The simulation is run for 25,000 time steps (though 15,000 were found to be adequate), with a time step of $\Delta t = 2.29847$ ps, and the solution is found to be entirely stable once again. The reflection plot of the circular patch antenna as a function of frequency is shown in Fig. 13. The results reported in [4] via the application of the symmetric and asymmetric Planar Generalized Yee (PGY) approaches, and those obtained by using the MoM [24], are also plotted in the same figure for the sake of comparison. The CFDTD results are seen to compare quite favorably with those obtained via the MoM; however, both the PGY (symmetric) and PGY (non-symmetric) methods are found to exhibit a slight downward shift in the resonant frequency. We also point out that the time step used in the PGY simulations Δt is 0.725 ps [4], which is one-third of that needed in the CFDTD simulations; hence, the latter offers considerable advantage in terms of computation time.

5.3.3. Annular Microstrip Resonator

In this example, we consider an annular microstrip resonator with orthogonal connecting lines, as shown in Fig. 14. This problem has been investigated by G. D’Inzeo, F. Gainini and R. Sorrentino [25] in 1980 by using the equivalent circuit theory. The inner and outer radii of the annular microstrip resonator are 4 mm and 7 mm, respectively. The deformed cells are distributed along the outer and inner boundaries of the annular microstrip resonator. The dimensions of the computational domain are $18.5 \times 18.5 \times 0.889$ mm³ and the volume is discretized into $61 \times 61 \times 7$ cells. The cell lengths Δx and Δy are 0.308333 mm in the region that contains the annular resonator, and 0.30 mm in the region outside it. A voltage source is used to excite the resonator at a distance of 4 cells away from the $y = 0$ boundary, and the measured voltage is sampled on the output line at a location 5 cells away from the $x = x_{max}$ boundary. The 3 dB cut-off frequency of the excitation source is 12 GHz. The simulation was run for 15,000 time steps, with a time step of $\Delta t = 0.3614$ ps, and the solution was found to be entirely stable. The scattering parameter S_{21} vs. frequency is shown in Fig. 15. Once again, good agreement with the experimental data given in [25] is observed. Furthermore, no instabilities were found, even when the program was tested up to 25,000 time steps.

5.3.4. Coupled Annular Microstrip Resonator

For the final example, we consider a coupled annular microstrip resonator, as shown in Fig. 16. The inner and outer radii of the coupled annular microstrip resonator are 4.75 mm and 5 mm, respectively. The relative permittivity of the substrate is 90. The dimensions of the computational domain are $11.25 \times 15.25 \times 2.25$ mm³ and the volume is discretized into $90 \times 122 \times 15$ cells. The cell lengths Δx and Δy are 0.125 mm in the x - y plane, and $\Delta z = 0.15$ mm in the z -direction. The width of the annular microwave resonator is equal to that of the two FDTD cells, as shown in Fig. 17. The deformed cells are distributed along the outer and inner boundaries of the annular microstrip resonator, as shown in Fig. 18. In the staircasing approximation, whether a

deformed cell is filled with the PEC or the substrate dielectric depends on the location of the central point of the cell.

A voltage source is used to excite the resonator at $x = 5.625 \text{ mm}$ and $y = 0.625 \text{ mm}$, and the measured voltage is sampled at $x = 5.625 \text{ mm}$ and $y = 13.375 \text{ mm}$. The 3 dB cut-off frequency of the excitation source is 5 GHz. The simulation was run for 40,000 time steps, with a time step of $\Delta t = 0.253 \text{ ps}$, and the solution was found to be entirely stable. The time domain voltage is plotted in Fig. 19. The E_z distribution and its contour plot on the substrate surface at $t = 384.79 \text{ ps}$ and $t = 641.32 \text{ ps}$ are plotted in Figs. 20 and 23, respectively. The scattering parameter S_{21} vs. frequency is shown in Fig. 24. Once again, good agreement with the experimental data is observed.

6. Conclusions

In this paper, we have described a conformal FDTD software package and have applied it to the simulation of several representative electromagnetic problems. An important feature of the present CFDTD technique is that it does not use the areas of the distorted cells; hence, the mesh generation is much simpler than that required by the other CFDTD techniques. The simulation data for all of the examples in this paper have been found to be in good agreement with the analytical and experimental results reported elsewhere. The CFDTD algorithm is computationally efficient because the time step is only slightly lower than that dictated by the Courant condition, rather than being pegged to the smallest size of the distorted cell.

REFERENCES:

- [1] K. S. Yee, "Numerical Solution of Initial Boundary Value Problems Involving Maxwell's Equations in Isotropic Media," *IEEE Transactions on Antennas and Propagation*, vol. 14, pp. 302-307, May 1966.
- [2] T. Itoh (Editor), *Time-Domain Methods for Microwave Structures*, IEEE Press, 1998.
- [3] W. D. Becker, P. H. Harms, and R. Mittra, "Time-Domain Electromagnetic Analysis of Interconnects in a Computer Chip Package," *IEEE Transactions on Microwave Theory and Techniques*, vol. 40, 1992, pp. 2155-2163.
- [4] S. Gedney, J. A. Roden, N. K. Madsen, A. H. Mohammadian, W. F. Hall, V. Shankar, and C. Rowell, "Explicit Time-Domain Solutions of Maxwell's Equations via Generalized Grids," in *Advances in Computational Electromagnetics: The Finite-Difference Time-Domain Method*, (A. Taflove, Editor) Boston, MA: Artech House, 1998.
- [5] R. Luebbers, F. Hunsberger, "FDTD for Nth Order Dispersive Media," *IEEE Transactions on Antennas and Propagation*, vol. 40, no. 11, pp 1297-1301, November 1992.
- [6] K. S. Yee and J. S. Chen, "The Finite-Difference Time-Domain (FDTD) and the Finite-Volume Time-Domain (FVTD) Methods in Solving Maxwell's Equations," *IEEE Transactions on Antennas and Propagation*, vol. 45, no.3, pp. 355-363, March 1997.
- [7] Monorchio, A., and R. Mittra, "Time-Domain (FE/FDTD) Technique for Solving Complex Electromagnetic Problems," *IEEE Microwave and Guided Wave Letters*, vol. 8, no.2, pp. 93-95, February 1998.
- [8] A. R. Bretones, R. Mittra, and R. G. Martin, "A Hybrid Technique Combining the Method of Moments in the Time Domain and FDTD," *IEEE Microwave and Guided Wave Letters*, vol. 8, no.8, pp. 281-283, August 1998.
- [9] R. Luebbers, F. Hunsberger, K. Kunz, "A Frequency Dependent Time Domain Formulation for Transient Propagation in Plasma", *IEEE Transactions on Antennas and Propagation*, vol. 39, no 1, pp. 29-34, January 1991.
- [10] S. Gedney, F. Lansing, and D. Rescoe, "A Full Wave Analysis of Passive Monolithic Integrated Circuit Devices Using a Generalized Yee Algorithm," *IEEE Trans. Microwave Theory Tech.*, vol. 44, 1996, pp. 1393-1400.
- [11] J.P. Berenger, "A perfectly matched layer for the absorption of electromagnetic waves," *J. Computat. Phys.*, Oct. 1994
- [12] M. Fusco, "FDTD Algorithm in Curvilinear Coordinates," *IEEE Transactions on Antennas and Propagation*, vol. 38, no.1, pp. 76-89, January 1990.
- [13] S. Dey and R. Mittra, "A Locally Conformal Finite Difference Time Domain (FDTD) Algorithm for Modeling Three-Dimensional Perfectly Conducting Objects," *IEEE Microwave and Guided Wave Letters*, vol.7, no.9, pp. 273-275, September 1997.
- [14] C. J. Railton, and J. B. Schneider, "An Analytic and Numerical Analysis of Several Locally Conformal FDTD Schemes," *IEEE Transactions on Microwave Theory and Techniques*, vol. 47, no.1, pp. 56-66, Jan. 1999.
- [15] T. G. Jurgens, A. Taflove, K. Umashankar, and T. G. Moore, "Finite-Difference Time-Domain Modeling of Curved Surfaces," *IEEE Transactions on Antennas and Propagation*, vol. 40, no. 4, pp. 357-366, April 1992.
- [16] Wenhua Yu, Raj Mittra, Dean Arakaki and Douglas H. Werner, "A Conformal Finite Difference Time Domain (CFDTD) Algorithm For Modeling Perfectly Conducting Objects," *The 16th Annual Review of Progress in Applied Computational Electromagnetics*, Monterey, CA, 2000.

- [17] Wenhua Yu and Raj Mittra, "Accurate Modeling of Planar Microwave Circuit Using Conformal FDTD Algorithm," *IEE Electronics Letters* (to be published).
- [18] S. D. Gedney, "An Anisotropic PML Absorbing Media for FDTD Solution of Fields in Lossy Dispersive Media," *Electromagnetics*, vol. 16, pp. 399-415, 1996.
- [19] Wenhua Yu, Manual for *Finite-Difference Time-Domain Solver*.
- [20] Wenhua Yu, S. Dey, and Raj Mittra, "On the Modeling Periodic Structures Using FDTD Method," *Microwave And optical Technology Letters*, vol.22, no.2, February 2000.
- [21] The Waite Group, *Visual Basic 6*, Waite Group Press, Corte Madera, CA 94925.
- [22] Mingwu Yang and Yinchao Chen, "AutoMesh: A automatically Adjustable, Non-Uniform, Orthogonal FDTD Mesh Generator," *IEEE Antennas and Propagation Magazine*, vol. 41, no.2, April 1999.
- [23] I. Wolff, "Applications of Finite-Difference Time-Domain Technique to Planar Microwave Circuit Design," in *Time-Domain Methods for Microwave Structures*, (T. Itoh, Editor) IEEE Press, 1998.
- [24] Zeland Software, 39120 Argonaut Way, Suite 499, Fremont, CA 94538.
- [25] G. D'Inzeo, F. Gainini, and R. Sorrentino, "Wide-Band Equivalent Circuits of Microwave Planar Networks," *IEEE Trans. Microwave Theory Tech.*, vol. 28, 1980, pp. 1107-1113.

Biographies

Wenhua Yu is a Research Associate in the Pennsylvania State University Department of Electrical Engineering. Dr. Yu received the BS degrees in Physics from Henan Normal University, XingXiang, in 1984, MS in Electrical Engineering from Beijing Broadcasting Institute, Beijing, in 1989, and PhD in Electrical Engineering from Southwest Jiaotong University, Chengdu, China, in 1994, respectively. Dr. Yu worked in Beijing Institute of Technology as a Postdoctoral Research Associate from February 1995 to August 1996. He worked in the Pennsylvania State University Department of Electrical Engineering as a Postdoctoral Research Associate from September 1996 to April 1999. He has published 25 technical papers and 20 proceeding articles. Dr. Yu has also developed two software packages for modeling MMIC, RF antennas and microstrip circuit components, waveguide and cavity. He is a Senior Member of the Institute of Electrical and Electronics Engineers.

His research interests include the areas of RF circuit design, packaged software development, computational electromagnetics, electromagnetic modeling and simulation of electronic packages, EMC analysis, frequency selective surfaces, microwave and millimeter wave integrated circuits, and satellite antennas.

Raj Mittra is Professor in the Electrical Engineering department of the Pennsylvania State University. He is also the Director of the Electromagnetic Communication Laboratory, which is affiliated with the Communication and Space Sciences Laboratory of the EE department. Prior to joining Penn State he was a Professor in Electrical and Computer Engineering at the University of Illinois in Urbana Champaign. He is a Life Fellow of the IEEE, a Past-President of AP-S, and he has served as the Editor of the Transactions of the Antennas and Propagation Society. He won the Guggenheim Fellowship Award in 1965, the IEEE Centennial Medal in 1984, and the IEEE Millennium medal in 2000. He has been a Visiting Professor at Oxford University, Oxford, England and at the Technical University of Denmark, Lyngby, Denmark. Currently, he serves as the North American editor of the journal AEÜ. He is the President of RM Associates, which is a consulting organization that provides services to industrial and governmental organizations, both in the U. S. and abroad.

His professional interests include the areas of RF circuit design, computational electromagnetics, electromagnetic modeling and simulation of electronic packages, communication antenna design including GPS, broadband antennas, EMC analysis, radar scattering, frequency selective surfaces, microwave and millimeter wave integrated circuits, and satellite antennas.

He has published over 500 journal papers and 30 books or book chapters on various topics related to electromagnetics, antennas, microwaves and electronic packaging. He also has three patents on communication antennas to his credit. For the last 15 years he has directed, as well as lectured in, numerous short courses on Electronic Packaging, Wireless antennas and Computational Electromagnetics, both nationally and internationally.

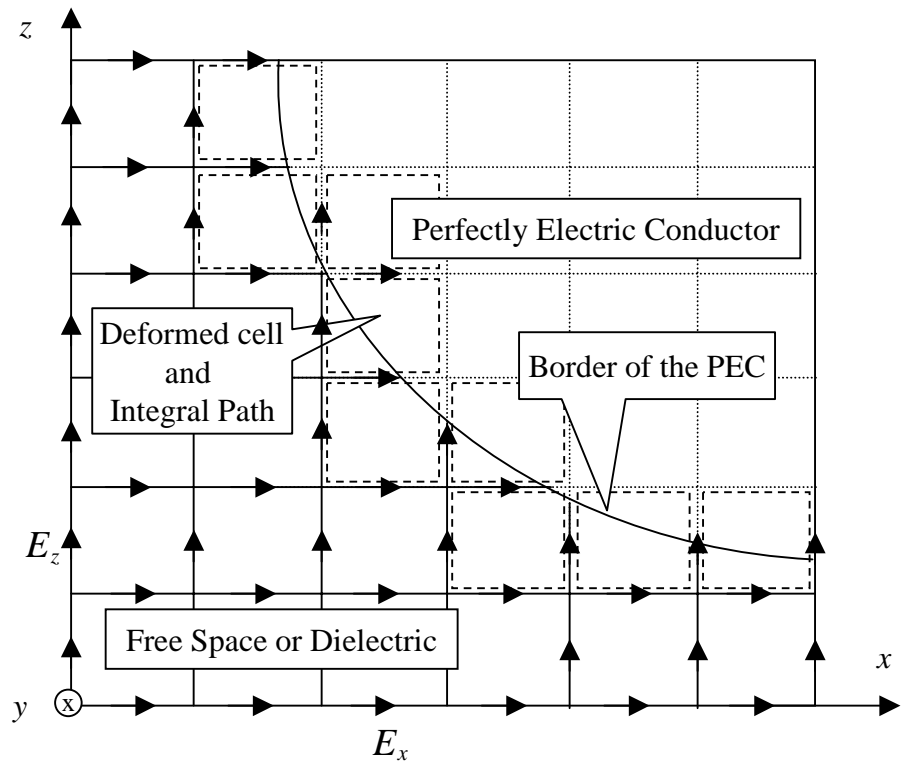


Fig. 1 Intersection between the FDTD mesh and a PEC surface in the x - z plane

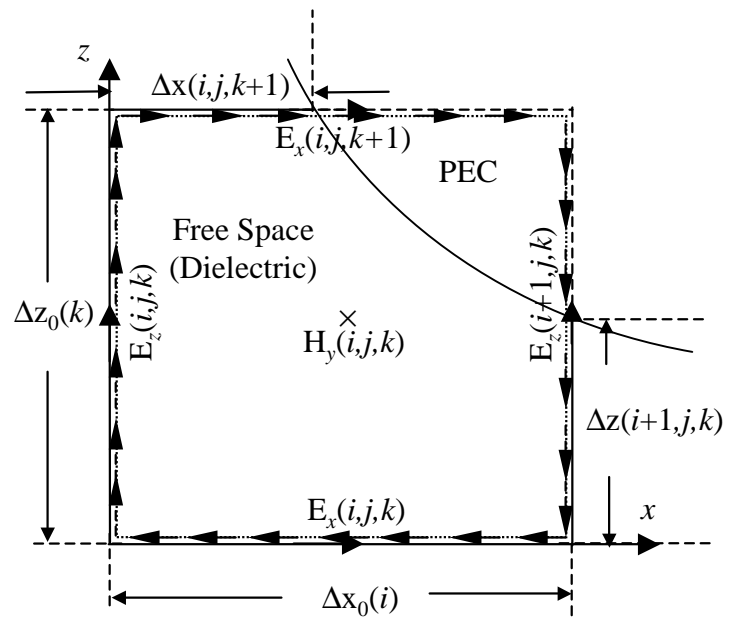


Fig.2 Contour path of the conformal FDTD in a deformed cell

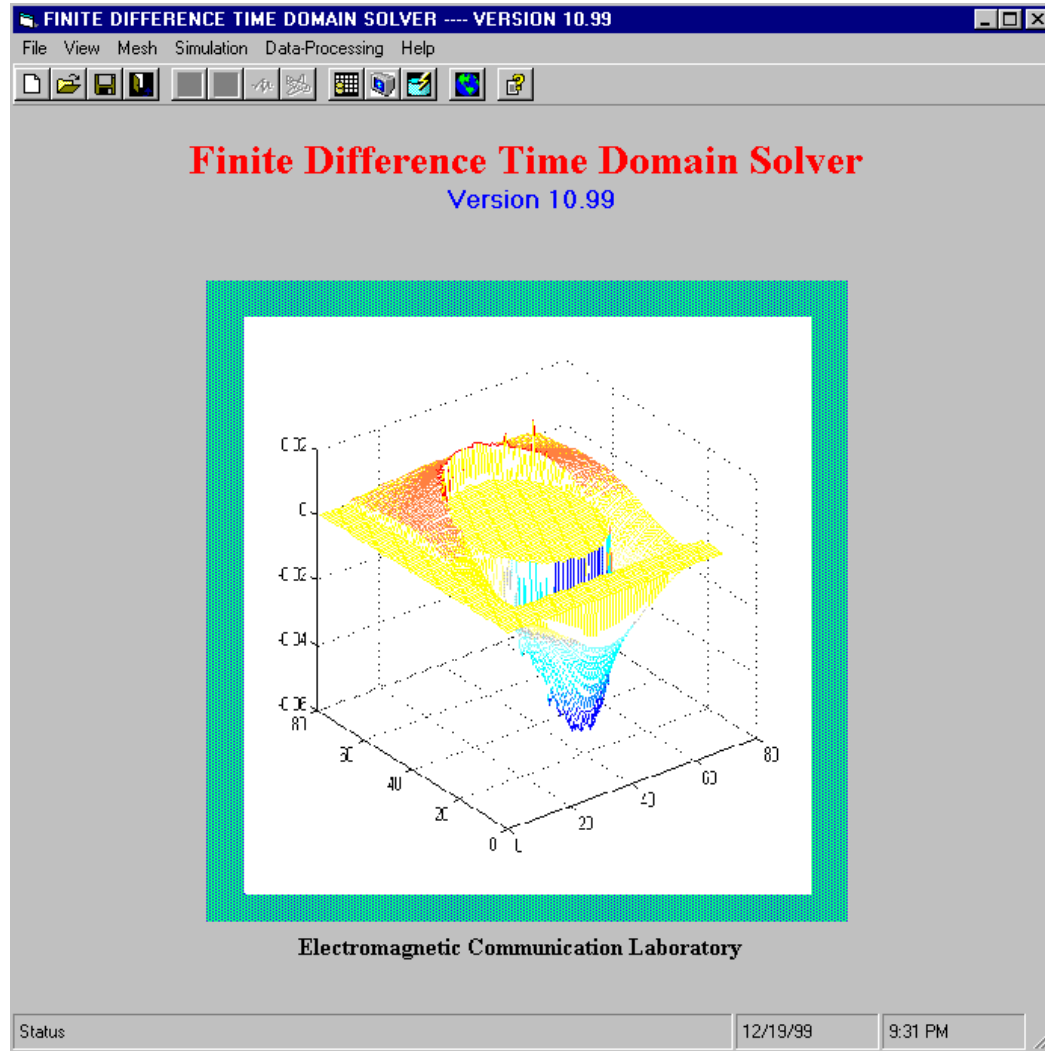


Fig. 3 Main page of the FDTD software Package

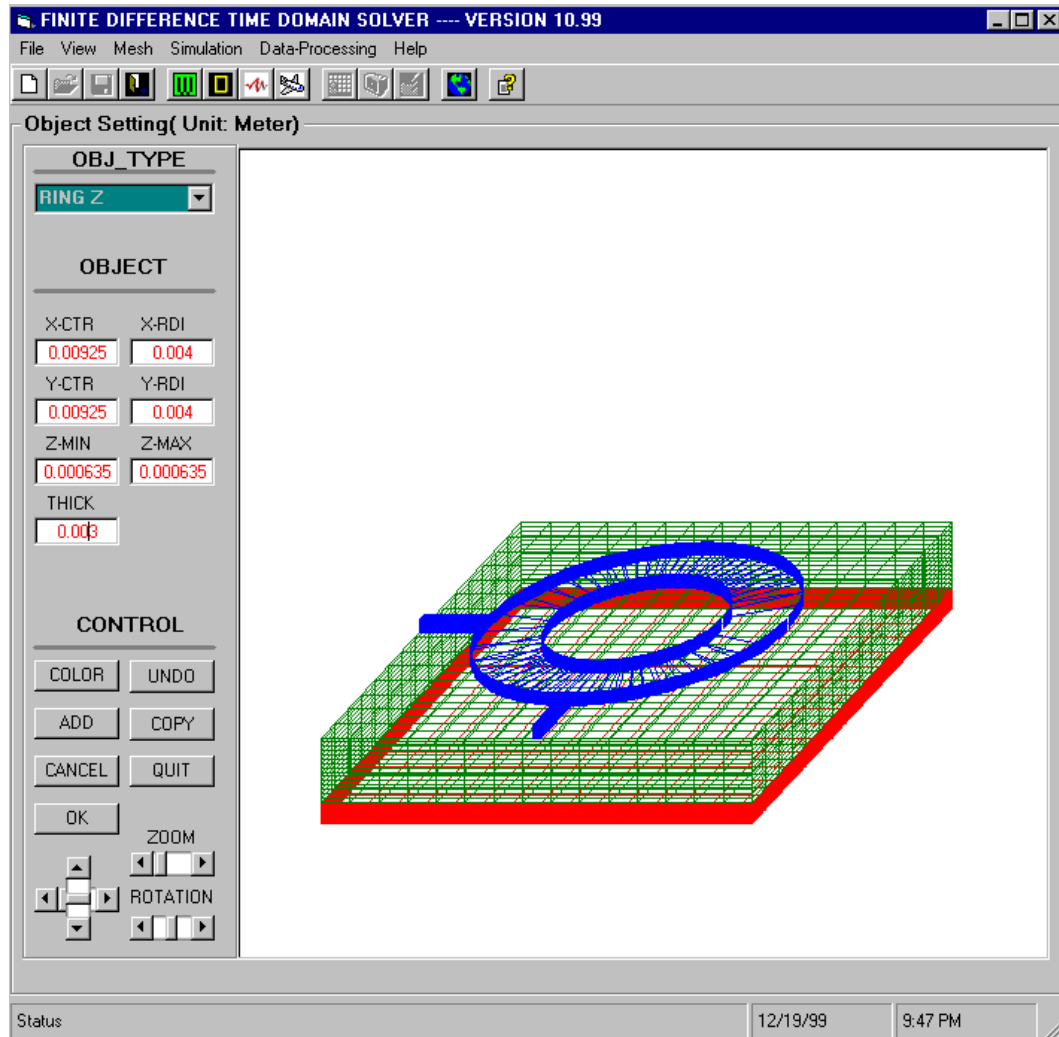


Fig. 4 Configuration of an annul microwave resonator

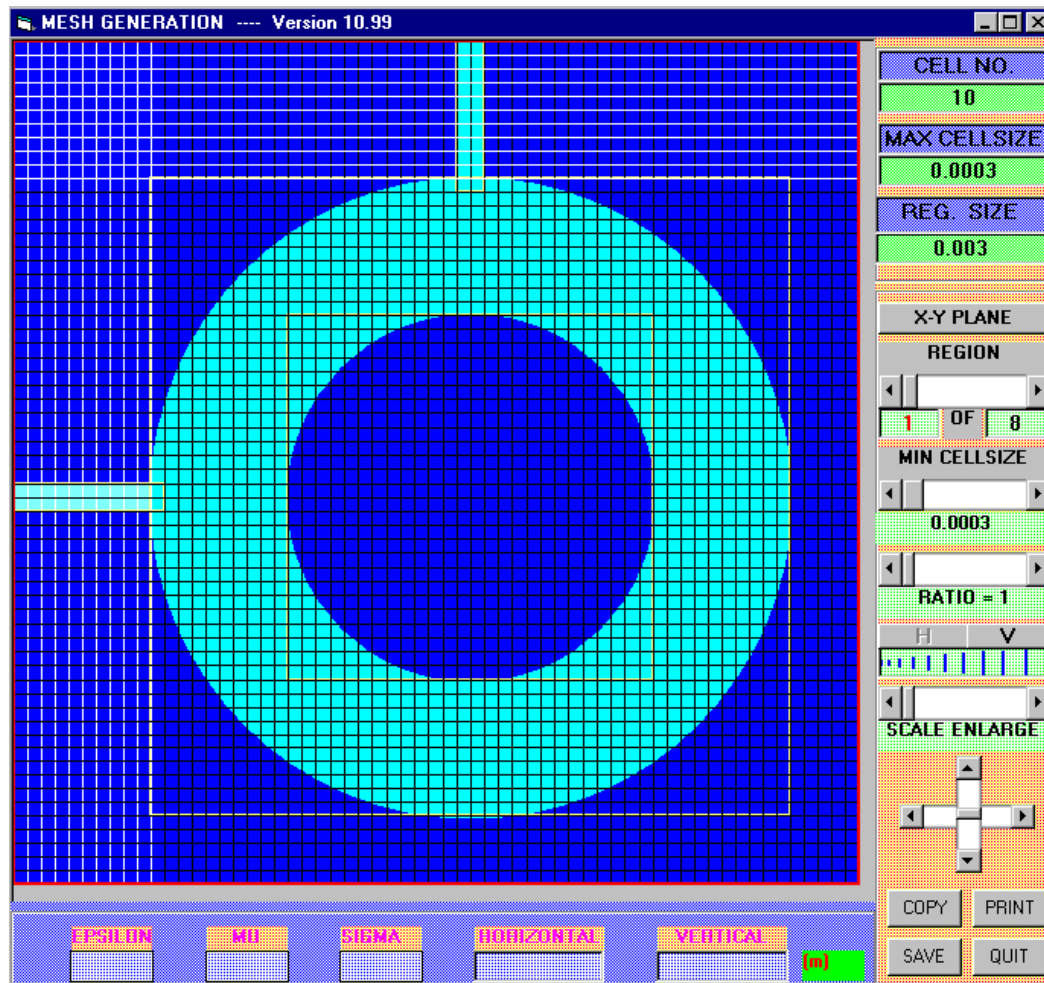


Fig. 5 Mesh configuration of an annul microwave resonator in the x - y plane.

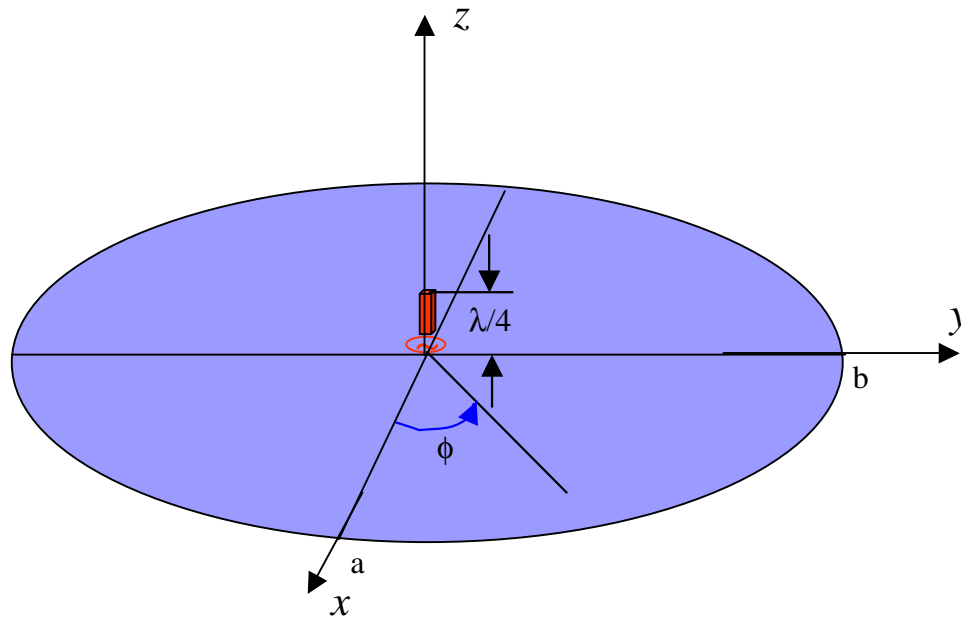


Fig. 6 A quarter wavelength monopole with an elliptic disk as the ground plane

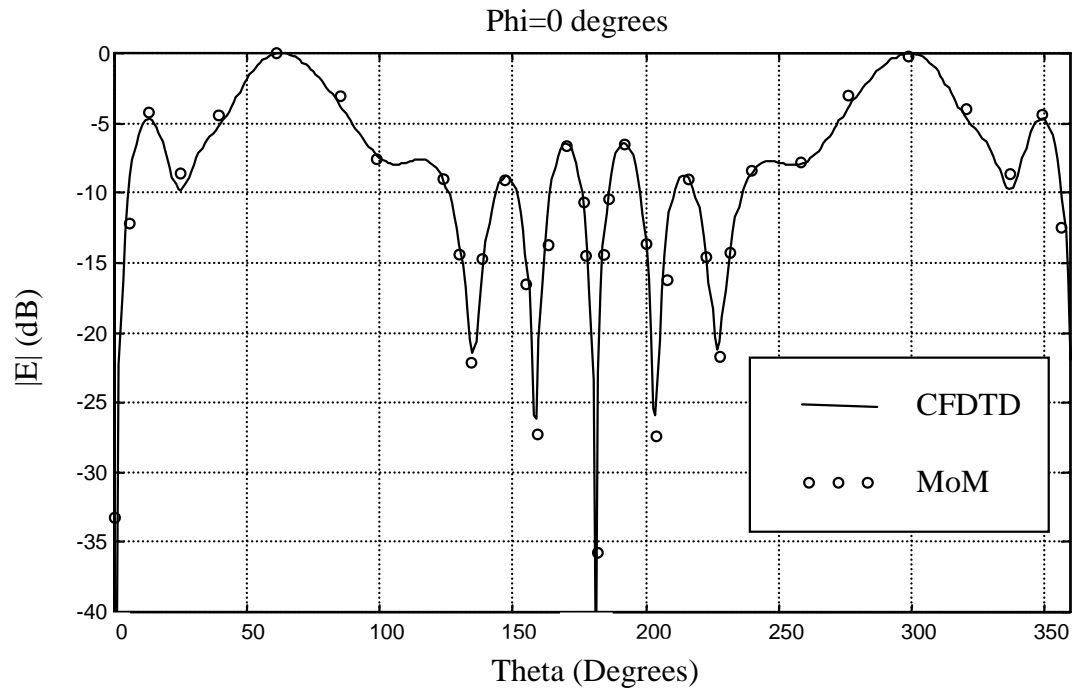


Fig. 7 Comparison of CFDTD and MoM solutions for the normalized radiated field ($\phi = 0^\circ$) by a $\lambda/4$ monopole located on an elliptic disk, with minor axis $a=1.5$ and major axis $b=1.7$ m. The frequency is 300 MHz.

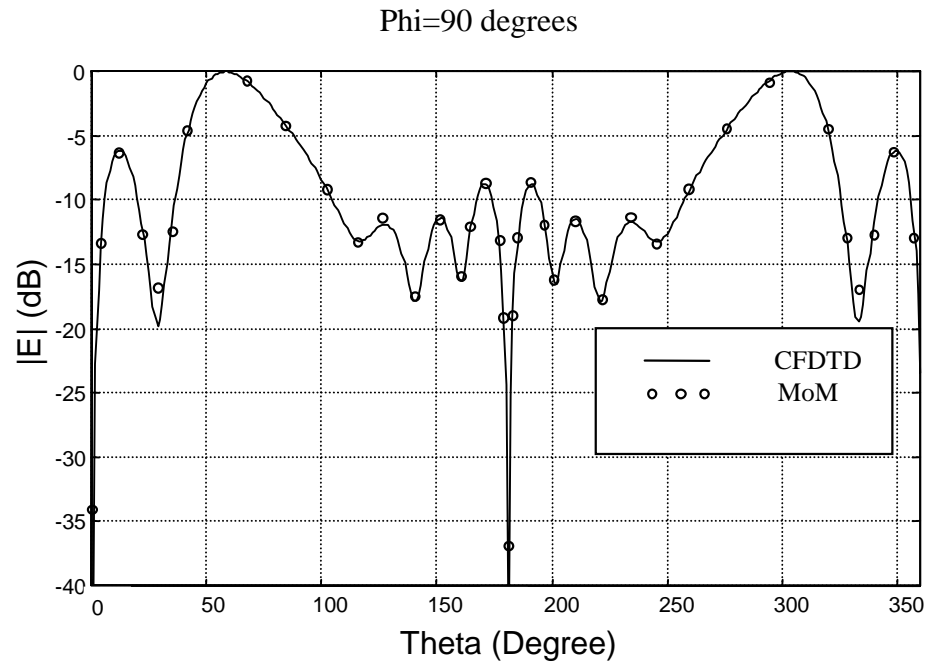


Fig.8 Comparison of CFDTD and MoM solutions for the normalized radiated field ($\phi = 90^\circ$) by a $\lambda/4$ monopole located on an elliptic disk, with minor axis $a=1.5$ and major axis $b=1.7$ m. The frequency is 300 MHz.

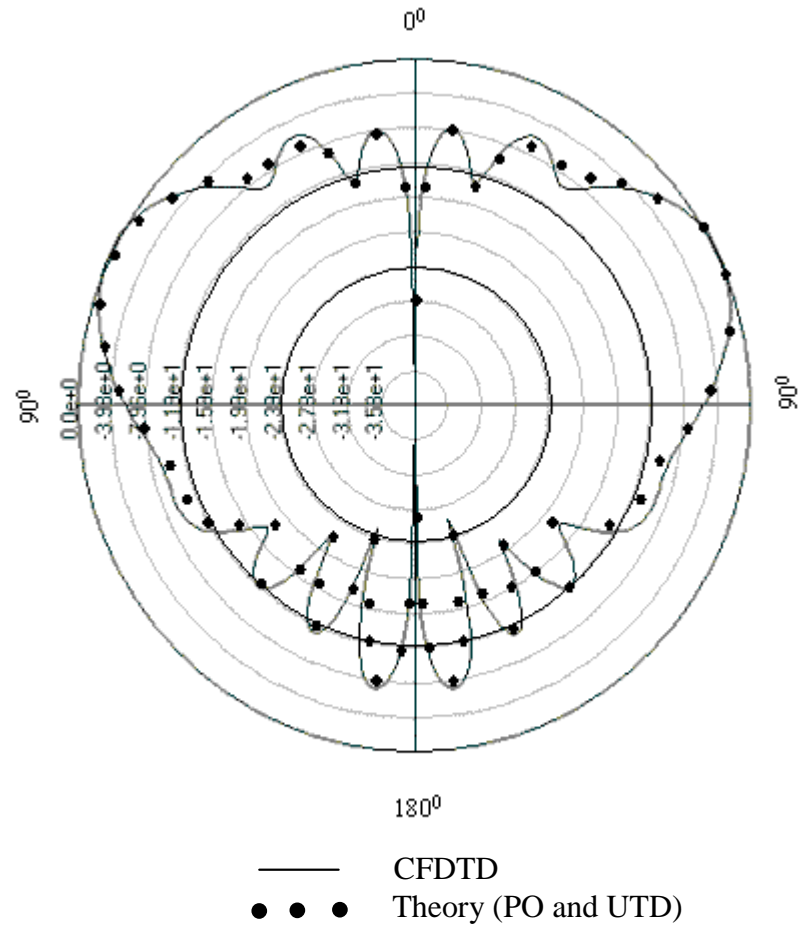


Fig. 9 Normalized far zone field pattern of a quarter wavelength monopole on a circular disk with $a=b=0.61$ m at a frequency of 1 GHz.

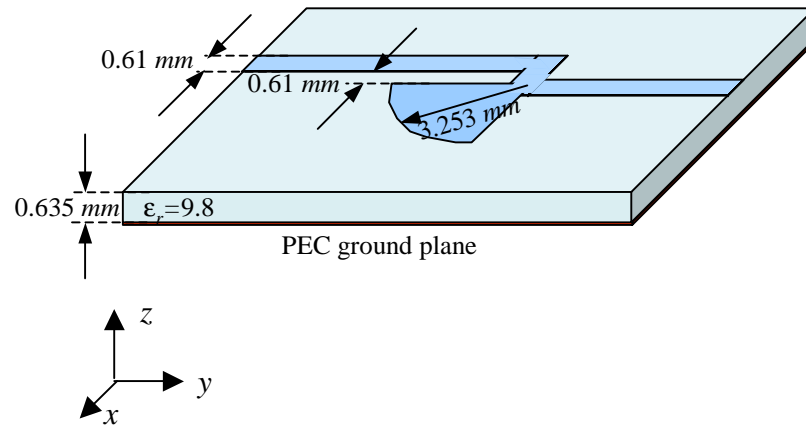


Fig.10 Microstrip line with a radial stub.

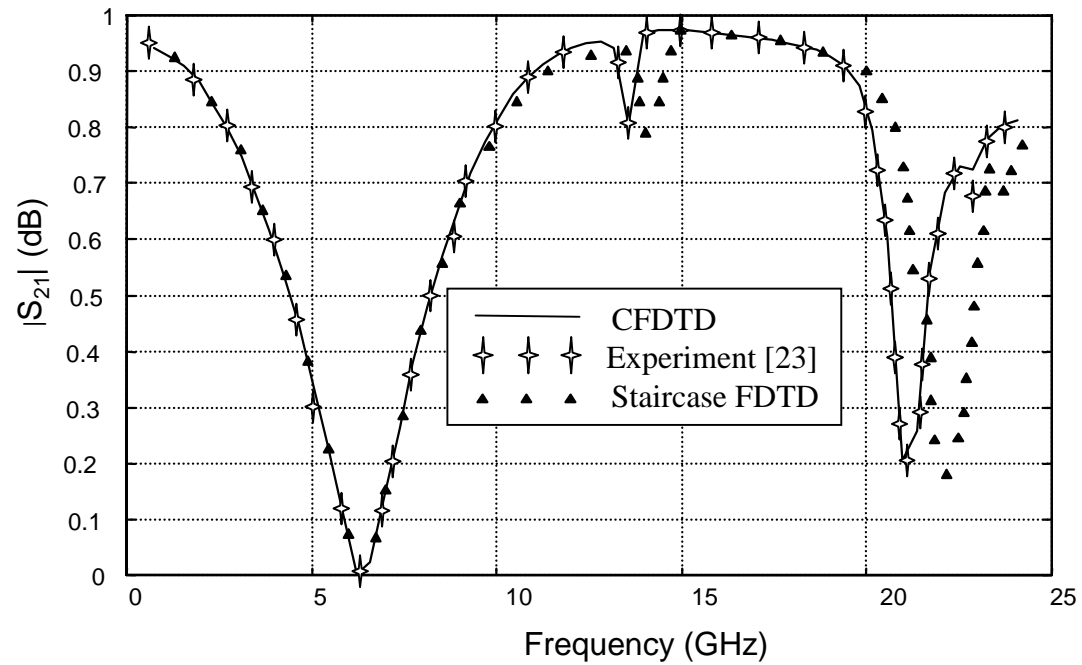
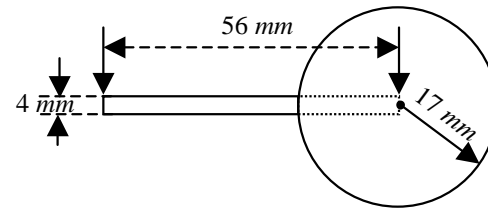
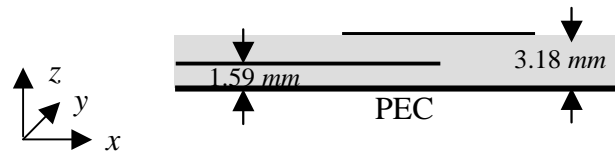


Fig. 11 Transmission coefficient of the microstrip line with a radial stub comparison of CFDTD and experimental results.



Top view



Side view

Fig. 12 Microstrip-coupled circular patch antenna. The microstrip line is located on a 1.59 mm substrate ($\epsilon_r = 2.62$) backed by a ground plane, and the patch antenna is printed on the same dielectric at a height of 1.59 mm , above the microstrip line.

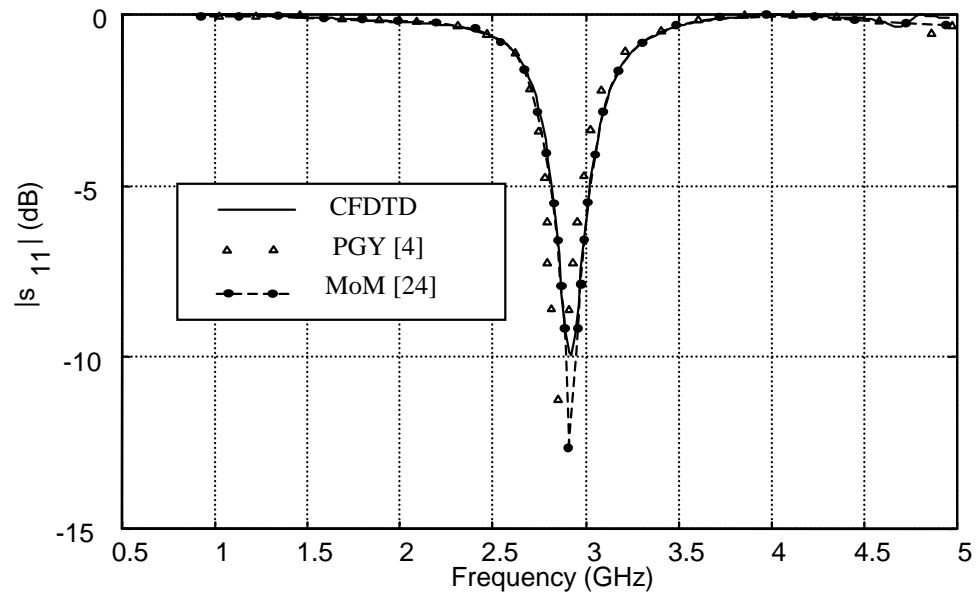


Fig. 13 Comparison of reflection loss of the microstrip-coupled circular patch antenna computed by using the CFDTD, the MoM and the PGY techniques.

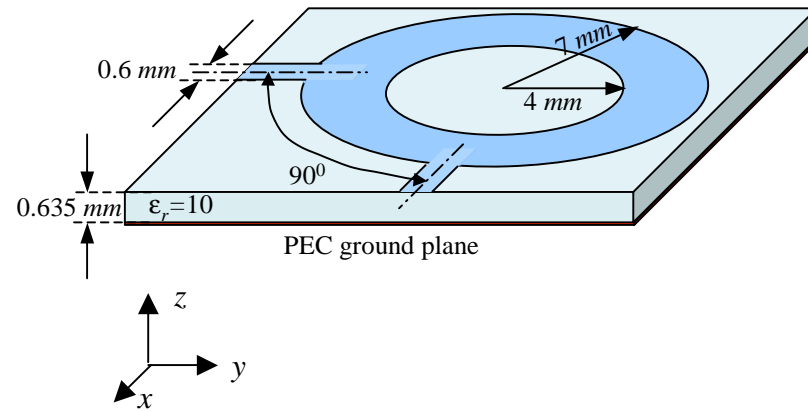


Fig. 14 Annular microstrip resonator.

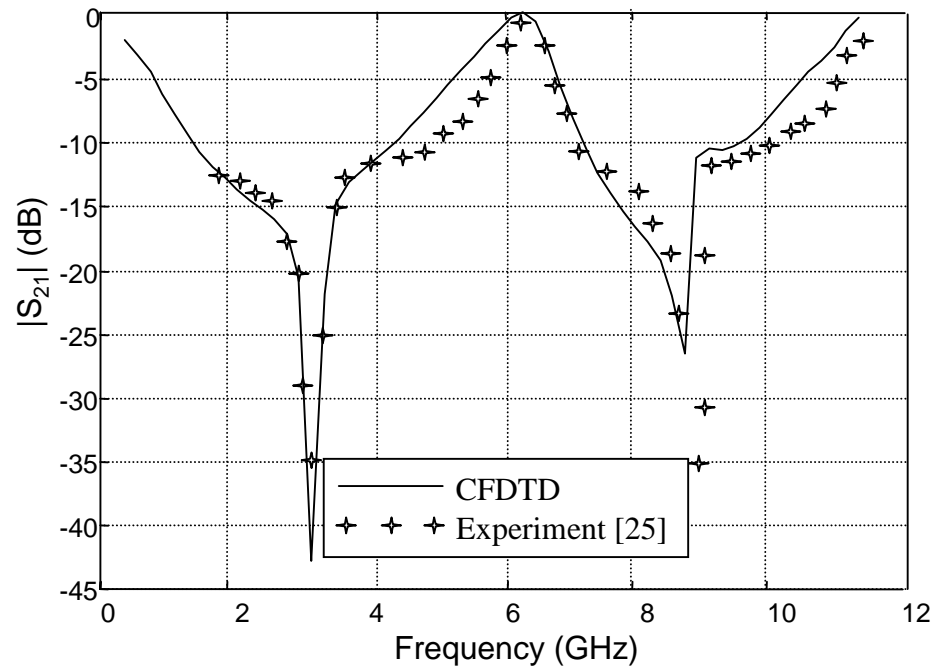


Fig. 15 $|S_{21}|$ vs. frequency characteristic of the annular microstrip resonator.

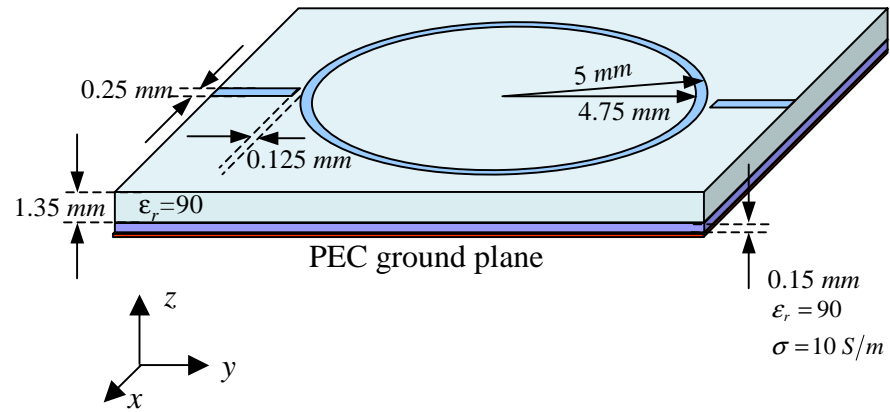


Fig. 16 Coupled annular microstrip resonator.

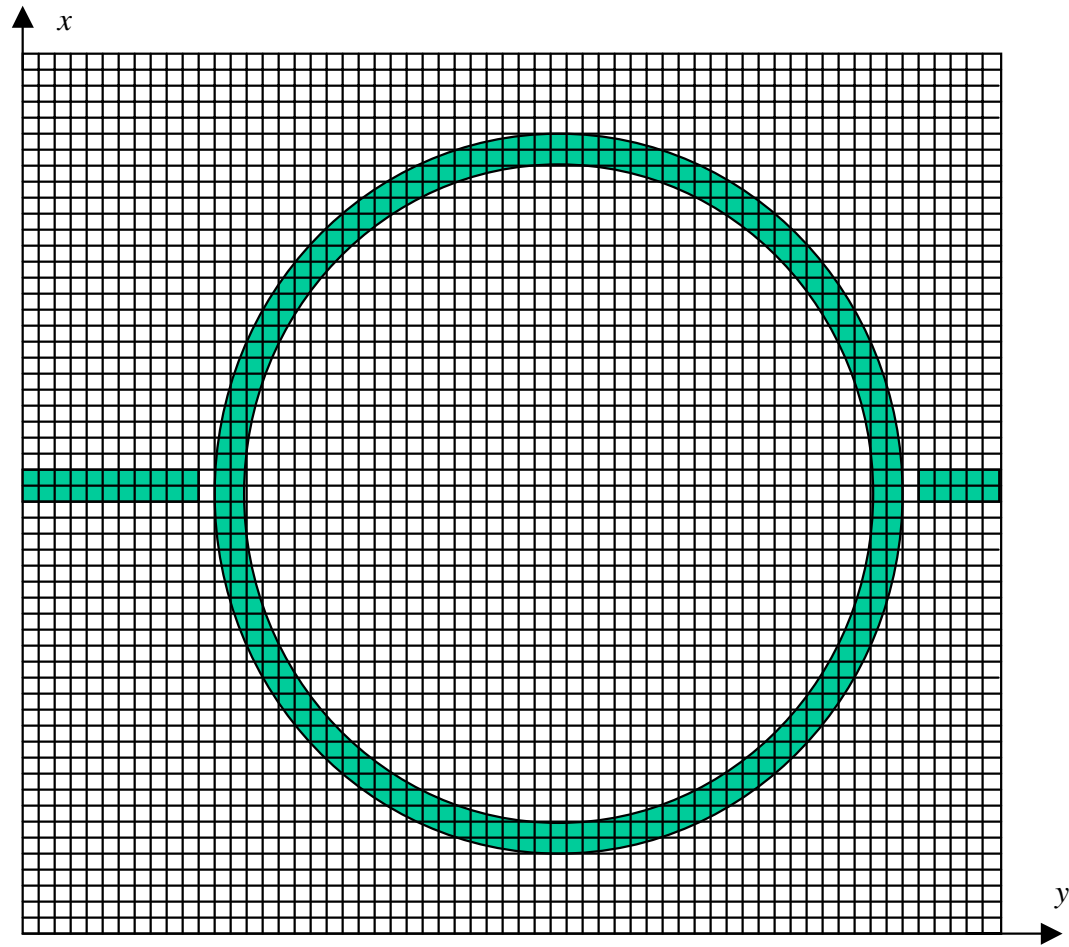


Fig. 17 Mesh configuration of the coupled annular microstrip resonator in the x - y plane.

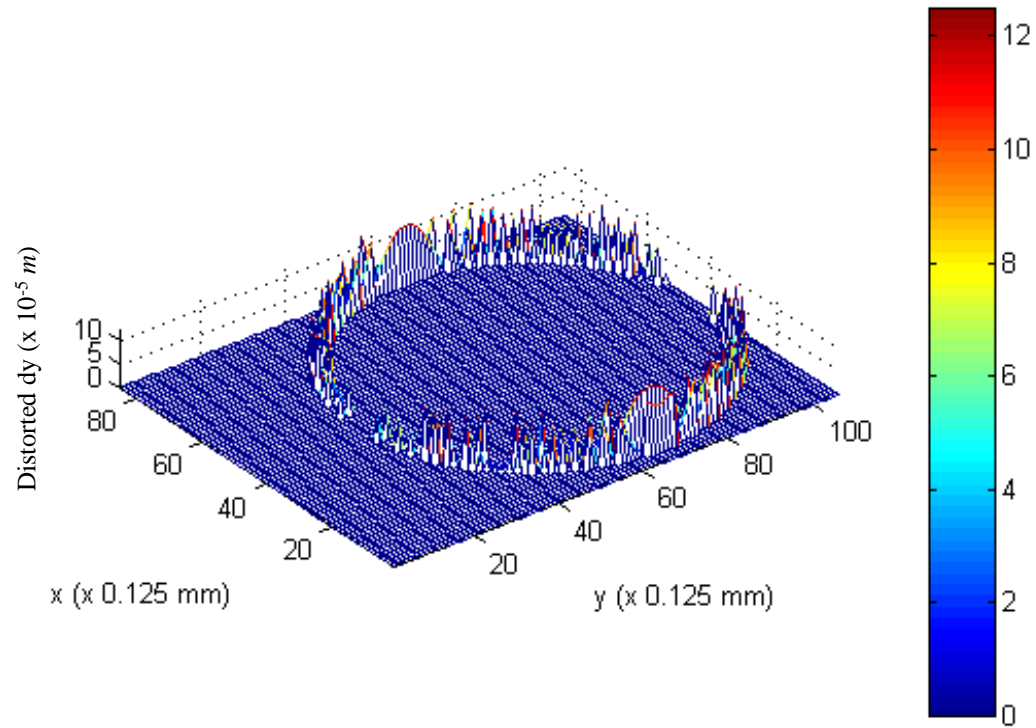


Fig. 18 Distribution of the deformed cell side lengths dy along the ring border.

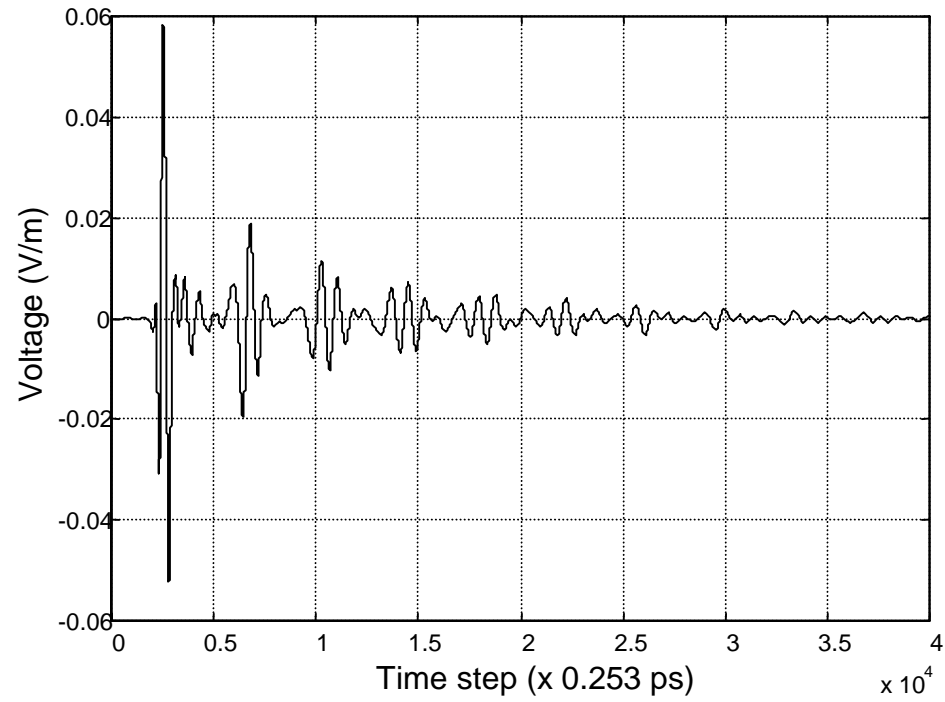


Fig. 19 Time domain voltage at the observation point of the transmission port.

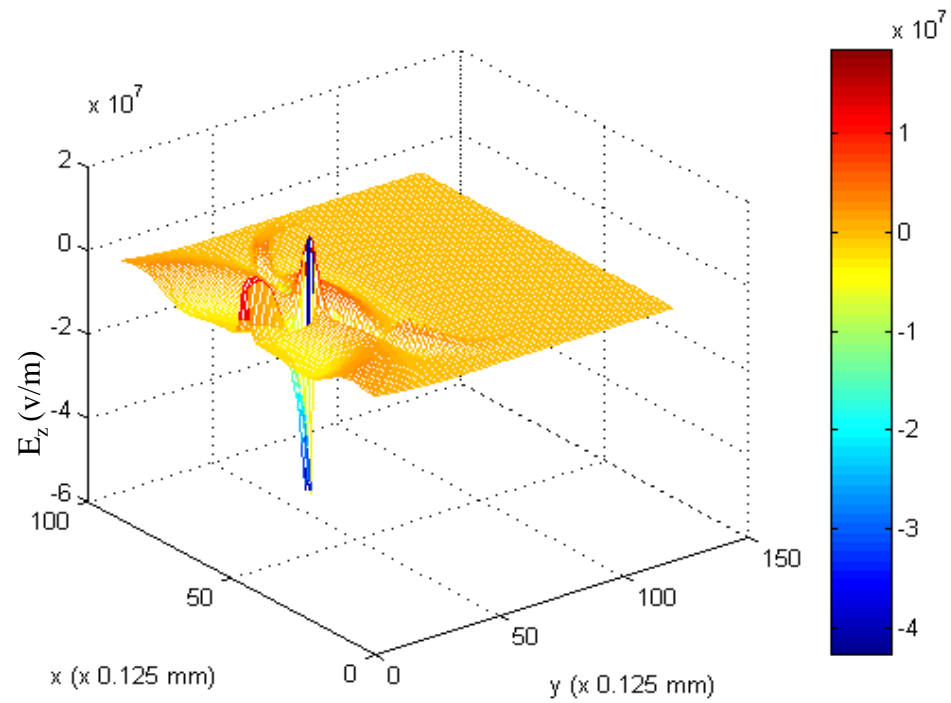


Fig. 20 E_z distribution on the substrate surface at $t = 384.79$ ps.

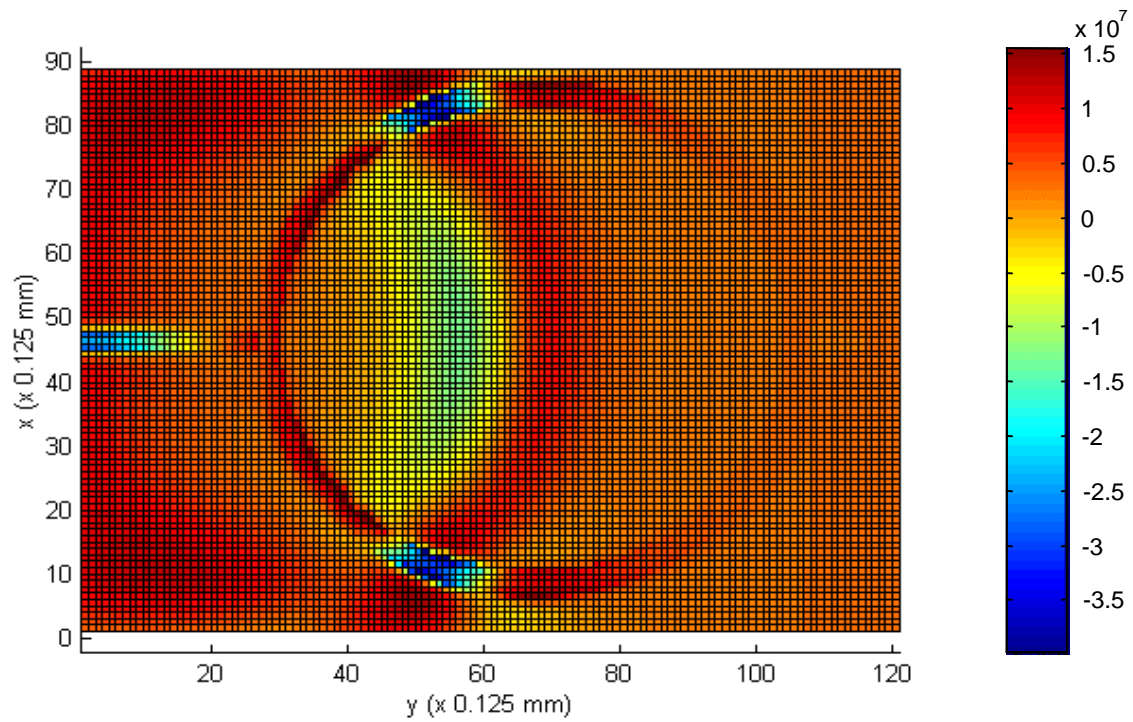


Fig. 21 Contour plot of E_z on the substrate surface at $t = 384.79$ ps.

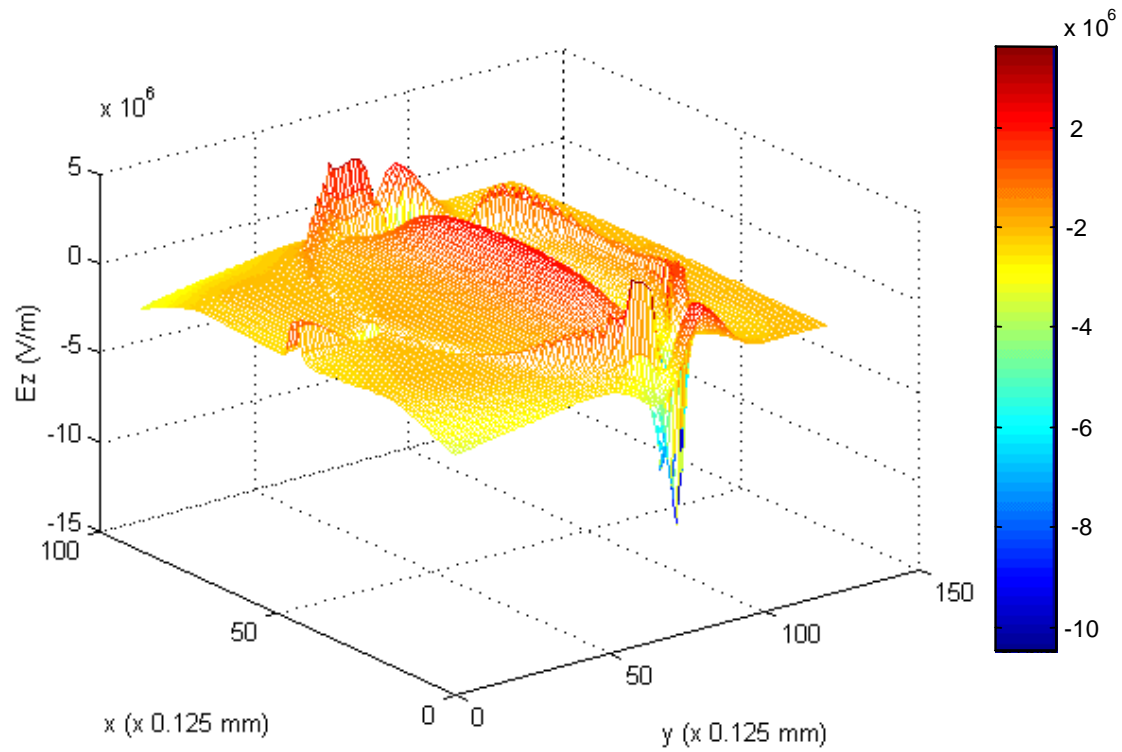


Fig. 22 E_z distribution on the substrate surface at $t = 641.32$ ps.

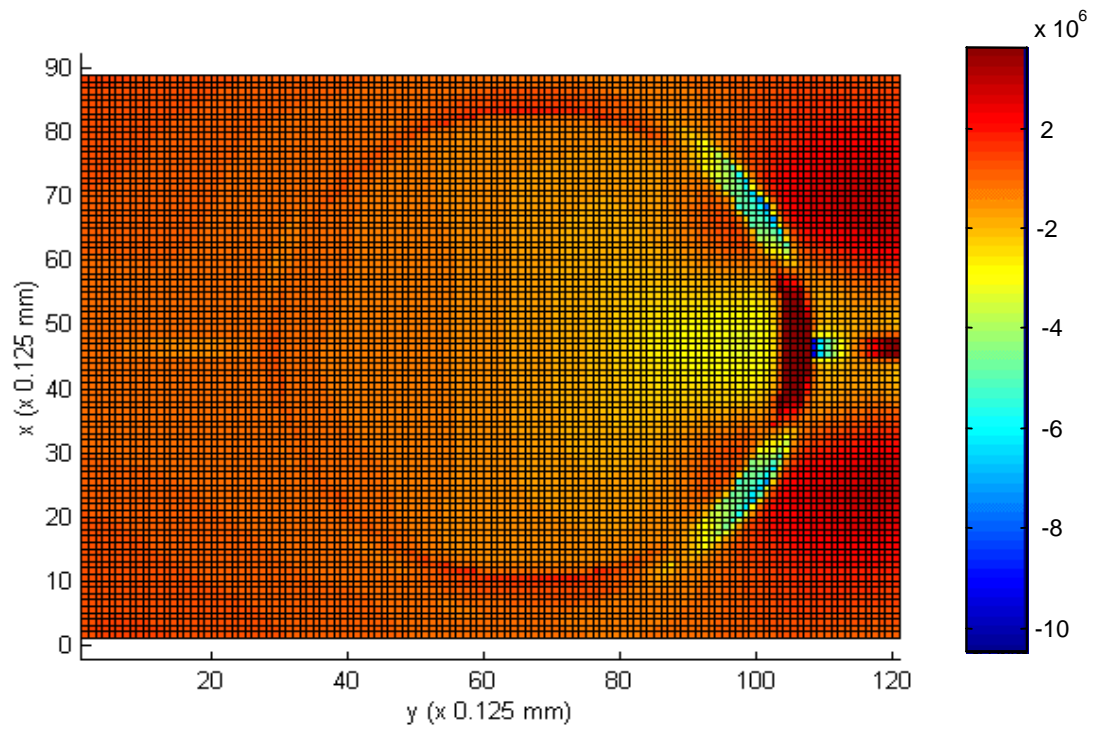


Fig. 23 Contour plot of E_z on the substrate surface at $t = 641.32$ ps.

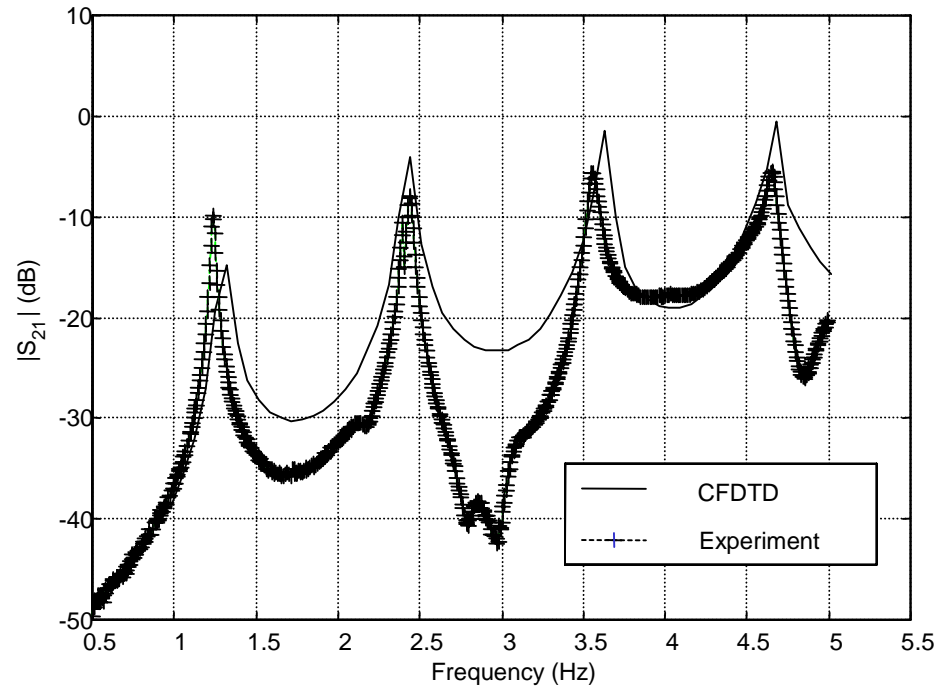


Fig. 24 $|S_{21}|$ vs. frequency characteristic of the coupled annular microstrip resonator.